



Facile Removal of Methylene Blue Using Carboxymethyl Cellulose Grafted Polyacrylamide/Carbon Black Nanocomposite Hydrogel

Seyed Jamaledin Peighambardoust¹ · Elmira Ghergherehchi¹ · Parisa Mohammadzadeh Pakdel¹ · Hassan Aghdasinia¹

Accepted: 23 October 2022 / Published online: 8 November 2022

© The Author(s), under exclusive licence to Springer Science+Business Media, LLC, part of Springer Nature 2022

Abstract

In the present work, novel pH-sensitive nanocomposite hydrogels were developed by grafting acrylamide onto carboxymethyl cellulose backbone (Hyd) using the free radical grafting polymerization method for the decontamination of methylene blue (MB) from an aquatic medium. Optimum values of weight percentage of acrylamide to total weight and content of carbon black nanoparticles based on removal efficiency were obtained at 75% and 7.5 wt%, respectively. The chemical structure, morphology, and thermal properties of synthesized adsorbents were characterized by FTIR, XRD, TGA, BET, and SEM methods. The removal efficiency under optimum conditions of pH 7, adsorbent dosage 1.5 g/L, contact time 60 min, dye initial concentration 10 mg/L, and temperature 25 °C were calculated to be 84.6 and 96.68% for Hyd and Hyd/CB, respectively. Kinetic and Equilibrium data were in good agreement with quasi-second-order and Langmuir models, respectively. With the rising temperature, the uptake of MB decreased, which implied the exothermic nature of the adsorption process.

Keywords Adsorbent · Carbon black · Methylene blue · Nanocomposite hydrogel · Wastewater treatment

Introduction

With the growth of the world population and the development of industries, the accessibility to healthy water is a global problem. Every day, a large volume of water is consumed in industries and is discharged into the environment without any treatment. Discharge of colored effluents from various industries such as textile, and paper leads to water resources causes severe problems in the natural ecosystem. It was estimated that around 7×10^5 tons of dyes are produced annually, and about 9 billion tons are discharged into water resources without any treatment [1]. Due to their complex structure, these pollutants suffer from low degradability and high stability to heat, light, and oxidizing agents. Methylene blue (MB) is a water-soluble cationic dye that causes severe problems in human health such as nausea, mental confusion, methemoglobinemia, eye burns, and vomiting [2]. Several dye removal technologies are proposed in countless research papers such as precipitation, chemical degradation, chemical

coagulation, and adsorption. Through these technologies, adsorption as an efficient, effective, and low-cost process has been examined over many years. The main restriction of this technology is the formation of secondary residues that need treatment before throwing away. Hydrogels are flexible three-dimensional polymeric networks with the capability of swelling in aquatic medium and adsorption of pollutants due to the presence of hydrophilic functional groups like carboxyl (COO^-), sulphonic ($-\text{SO}_3\text{H}$), hydroxyl ($-\text{OH}$), and amide ($-\text{CONH}$) [3]. Physical and chemical crosslinking methods were used to prepare these materials to avoid their dissolving in the water [4]. Physically crosslinked hydrogels have low mechanical strength so chemical crosslinking is the best method to prepare hydrogels, especially for wastewater treatment application. The reaction of functional groups, chemical grafting reaction, free radical polymerization, and high energy irradiation are common methods of chemical crosslinking of hydrogels [5]. To develop low-cost, biodegradable, and biocompatible hydrogels, different biopolymers like chitosan, carboxymethyl cellulose, alginate, starch, salecan, carrageenan, and gelatin are used [6]. Among derivatives of cellulose, carboxymethyl cellulose (CMC) has high solubility due to the replacement of some of $-\text{OH}$ group by the carboxyl. Due to the presence of hydroxyl and carboxyl

✉ Seyed Jamaledin Peighambardoust
j.peighambardoust@tabrizu.ac.ir

¹ Faculty of Chemical and Petroleum Engineering, University of Tabriz, Tabriz 5166616471, Iran

groups, CMC can be effectively utilized for removing cationic dyes and heavy metals [3]. Besides low thermal and mechanical properties, CMC hydrogels suffer from low specific surface area and low functionality. So, to enhance the performance of neat CMC hydrogels various strategies are developed such as blending, grafting, and using nanoparticles. Grafting of multiple monomers such as acrylic acid, methyl methacrylate, acrylamide, N-Isopropylacrylamide, itaconic acid (IA), and 2-acrylamido-2-methylpropane sulfonic acid (AMPS) on CMC backbone by free radical polymerization method has been reported in literatures [3, 7–10]. Peighambarous et al. indicated that the CMC based hydrogel containing acrylamide can efficiently adsorb malachite green dye [9]. Sinha et al. synthesized CMC-g-AMPS/Fe/Al/AC composite hydrogels for remediation of fluoride (F^-) ions from aqueous solution. They revealed that the maximum removal efficiency of F^- is 84.67% which is occurs at pH of 6 [11]. To further enhancement of grafting networks, various nanomaterials such as clays [12], graphene oxide [10, 13], activated carbon [14], carbon black [15], and multiwall carbon nano-tube [16] are used. Incorporation of these nanomaterials not only enhances mechanical and thermal properties but also promotes swelling and adsorption capability. To enhance the antibacterial performance of hydrogels some metal-based nanoparticles can be incorporated into polymer matrix such as silver. Khan et al. synthesized silver nanoparticles using sulfonated carboxymethyl cellulose as a biocompatible stabilizer and a non-toxic reducing agent. The obtained results showed that silver nanoparticles have a good antimicrobial performance against Gram-positive *B. subtilis* and Gram-negative *E. coli* bacterial strains [17]. Makhado et al. prepared xanthan gum-cl-poly(acrylic acid)/o-MWCNTs nanocomposite hydrogel to remove MB from aqueous solution. The adsorption data of synthesized adsorbents follow quasi second order and Langmuir models. They showed that the addition of o-MWCNTs enhances the reusability of hydrogel in successive adsorption–desorption cycles [18]. Makhado et al. synthesize xanthan gum-cl-pol(acrylic acid)/rGO nanocomposite hydrogels by free radical polymerization using microwave irradiation method to remove MB and methyl violet from aqueous solution. They showed that incorporation of rGO improves swelling and removal efficiency. The equilibrium adsorption data of both dyes were well fitted with the Langmuir isotherm model [19]. Wang et al. prepared chitosan/montmorillonite nanocomposite hydrogel to remove Pb^{2+} from aquatic medium. The results of XPS analysis showed that ion exchange is the main mechanism of Pb^{2+} adsorption [20]. For developing hydrogels with capability of photocatalytic degradation of dyes using UV light, TiO_2 and ZnO nanoparticles can be employed [21, 22]. However, their use in the industrial scale is a challengeable issue. In recent years, carbon base materials have attracted the attention of many researchers

due to their excellent surface area, abundance, and electrical characteristics [23]. One of the best carbon base nanomaterials in the preparation of nanocomposite hydrogels is carbon black (CB) which is generated from incomplete combustion of hydrocarbons. CB as an industrial carbon material can be used in wastewater treatment applications due to the existence of carboxyl, carbonyl, and hydroxyl functional groups in its structure. Structurally, CB consists of two parts graphitic and amorphous. In the graphitic domain, layers of hexagonal rings of carbon which is called basic structural unit (BSU) stacked together with interlayer distance of 0.35 nm [24]. Amorphous core is more or less concentrically surrounded by units of carbon layers [24, 25]. Another attractive carbon-base nanomaterial that gained the attention of researchers is graphene oxide (GO). GO has a layered structure showing high thermal stability, good mechanical strength, and chemical properties. GO is a good candidate to remove pollutants from wastewater due to high specific surface area and presence of functional groups like epoxy, hydroxyl, and carboxyl [26]. However, the disadvantages of GO in comparison with CB are its high cost and difficulties in production.

In this work, poly(acrylamide) grafted on carboxymethyl cellulose hydrogels were synthesized by free radical polymerization method using potassium persulfate (KPS) as an initiator and N, N'-methylene bisacrylamide (MBA) as a chemical cross-linker for remediation of methylene blue dye from the aquatic medium. To improve the removal efficiency of CMC-based hydrogel, various contents of CB nanoparticles are incorporated into the hydrogel matrix. The impact of different adsorption conditions such as pH, initial concentration, dose, temperature, and contact time on removal efficiency was precisely studied to achieve optimum conditions. To assess the chemical structure, thermal stability, and morphology of synthesized hydrogels, Fourier-transform infrared spectroscopy (FTIR), X-ray diffraction analysis (XRD), Thermogravimetric analysis (TGA), Brunauer, Emmett, and Teller (BET), and scanning electron microscopy (SEM) were performed. Also, kinetics and isotherm models were evaluated to discover the mechanism of adsorption.

Materials and Methods

Materials

Potassium persulfate (KPS, 98.0%) was purchased from Samchun chemical Co, Korea. Sodium carboxymethyl cellulose (Na-CMC, average $M_w \sim 90,000$), Acrylamide (AAM, 99%), and N,N'-methylene bisacrylamide (MBA, 99.5%) were obtained from Merck, Germany. Sodium hydroxide (NaOH), hydrochloric acid (HCl, 37%), sodium chloride (NaCl), and calcium chloride ($CaCl_2$) were bought from

Merck, Germany. Carbon black with an average particle size of 0.042 microns was purchased from Exir.co, Australia. It is a byproduct of acetylene production from natural gas. Methylene blue (MB) was obtained from Mojallali reagent chemical Co. (Iran, Tabriz). All reactants possessed analytical grade and deionized water was used throughout the work.

Synthesize of Hydrogel Samples

At first, 1.0 g of CMC powder was dissolved in 20 mL deionized water in a 250 mL four-necked round bottom flask equipped with a stirrer, a thermometer, nitrogen gas inlet, nitrogen gas outlet tubes, and a reflux condenser to obtain a viscous solution. Under the atmosphere of N₂, the temperature of the CMC solution was raised to 70 °C. After 30 min of N₂ purging, 0.1 g of the KPS was added to this sticky solution to produce CMC radicals and vigorously stirred. After 10 min, the mixture of monomer and cross-linker was charged to the flask. After 3 h, the obtained gel product was cut into small pieces and washed with distilled water several times to eliminate unreacted monomer, initiator, and soluble polymers. Afterward, the gel pieces were placed in an oven at 70 °C for 24 h until they were completely dried. The dried hydrogel was ground into the powder and sifted through 40–80 sieves for the removal of MB. The preparation method of nanocomposite hydrogels is identical to the hydrogel synthesis method just a determined amount of CB was added to the monomer and cross-linker solution and sonicated for half of 1 h then this suspension solution was discharged to the reaction flask. The feed composition of synthesized hydrogels is tabulated in Table 1.

Characterizations

FTIR analysis of CMC, AAm, Hyd, and Hyd/CB nanocomposite hydrogel was performed by the FTIR spectrometer

(Tensor 27, Bruker, Germany) operating at wavenumbers of 400 to 4000 cm⁻¹. The surface morphology of CMC before and after graft copolymerization with P(AAm), CB, Hyd/CB nanocomposite hydrogel was demonstrated by scanning electron microscopy (SEM, MIRA3, TESCAN, Brno, Czech Republic) under the voltage of 15 kV. The samples were made conductive by coating them with gold by sputtering after fracturing them in liquid nitrogen. To evaluate the thermal stability of CMC, Hyd, and Hyd/CB nanocomposite hydrogel, a thermogravimetric analyzer (TGA-PL, TGA 1500, Canada) was used operating at a heating rate of 10 °C/min and temperature range of 25–900 °C under nitrogen atmosphere. X-ray diffraction (XRD) analysis was used to find out the crystalline or amorphous nature of CMC, CB, Hyd, and Hyd/CB by (Krisalloflex D500, Siemens, Germany) diffractometer equipped with CuKα irradiation (λ = 1.5406 Å) operating at 40 kV and 25 mA over the scanned range of 4°–80° with a scan step of 0.05°. N₂ adsorption–desorption isotherm plots were obtained at 77 K using by gas sorption instrument (A sap 2020, Micrometrics, USA) to calculate specific surface area, mean pore diameter, and total pore volume of CB, Hyd, and Hyd/CB.

Dye Adsorption Study

The impact of initial concentration, dose, pH, contact time, and temperature on the removal efficiency was studied in batch mode. Before placing flasks on a thermostatic shaker, a determined amount of adsorbent was charged into flasks containing 50 mL of methylene blue solution. After ending the adsorption process, the dye solution was centrifuged and the final concentration of dye was measured by UV–Visible spectrophotometer (Hanon Instruments Co, Model I3, China) at a maximum absorption wavelength of methylene blue (λ_m = 664 nm). The equilibrium adsorption capacity of adsorbent (q_e(mg/g)) and removal efficiency are computed by Eqs. 1 and 2, respectively.

$$q_e = \frac{(C_i - C_e)}{m} V \quad (1)$$

$$\text{Removal (\%)} = \frac{C_e - C_i}{C_i} \times 100 \quad (2)$$

C_i, C_e, V (L), and m (g) are the initial and equilibrium concentrations of dye, the volume of the MB solution, and the amount of adsorbent, respectively. All adsorption experiments were performed three times and the mean standard deviation was reported as the error.

Table 1 The feed composition of adsorbent samples

Adsorbent codes	Weight percent-age of AAm to total weight (wt%)	KPS (g)	MBA (g)	CB (wt%)
Sample (1)	50	0.1	0.02	0
Sample (2)	67	0.1	0.02	0
Sample (3)	75	0.1	0.02	0
Sample (4)	80	0.1	0.02	0
Sample (5)	75	0.1	0.02	2.5
Sample (6)	75	0.1	0.02	5
Sample (7)	75	0.1	0.02	7.5
Sample (8)	75	0.1	0.02	10
Sample (9)	75	0.1	0.02	12.5
Sample (10)	75	0.1	0.02	15

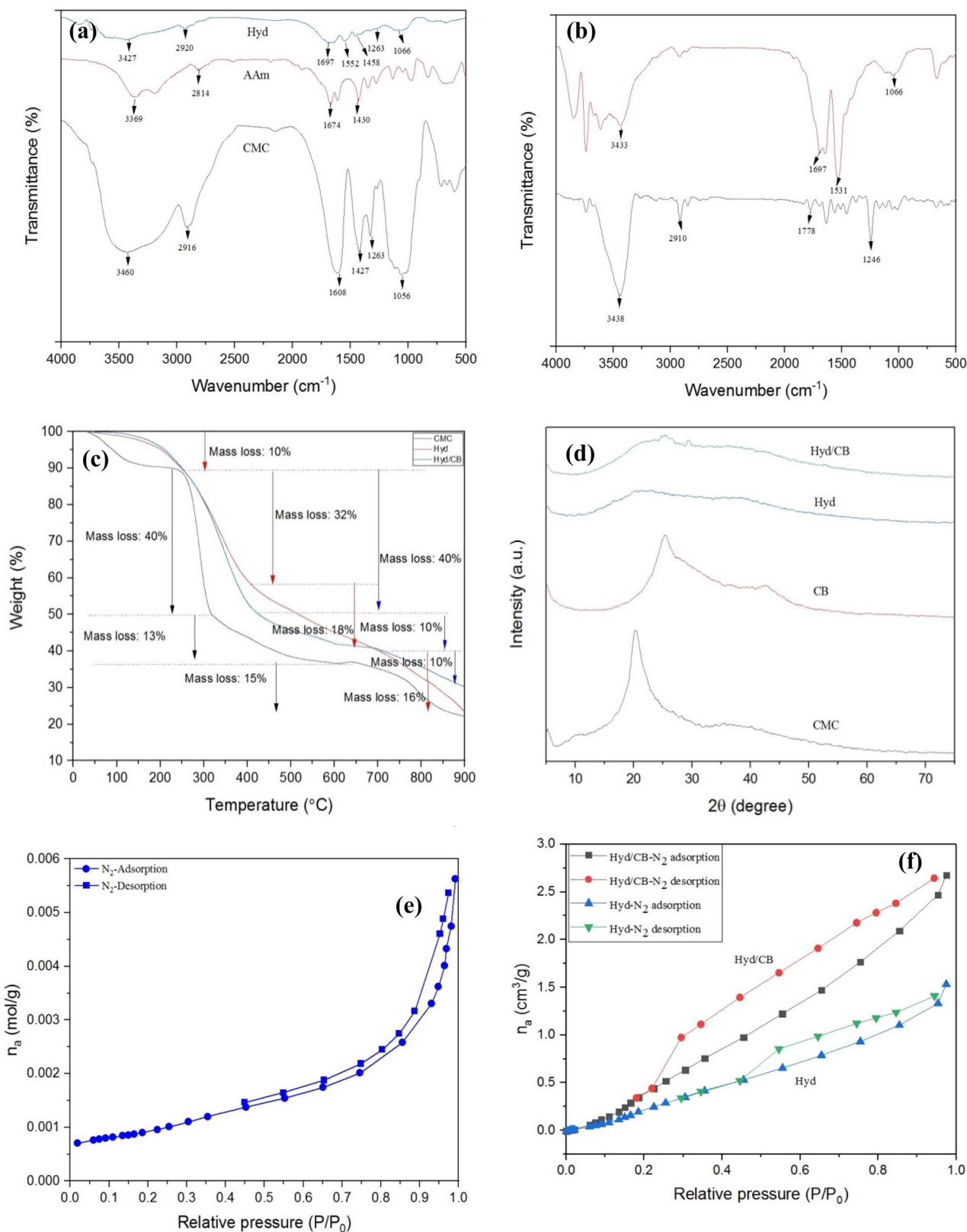


Fig. 1 Analyses of **a, b** FTIR, **c** TGA, **d** XRD, **e** BET of CB, and **f** BET of Hyd and Hyd/CB

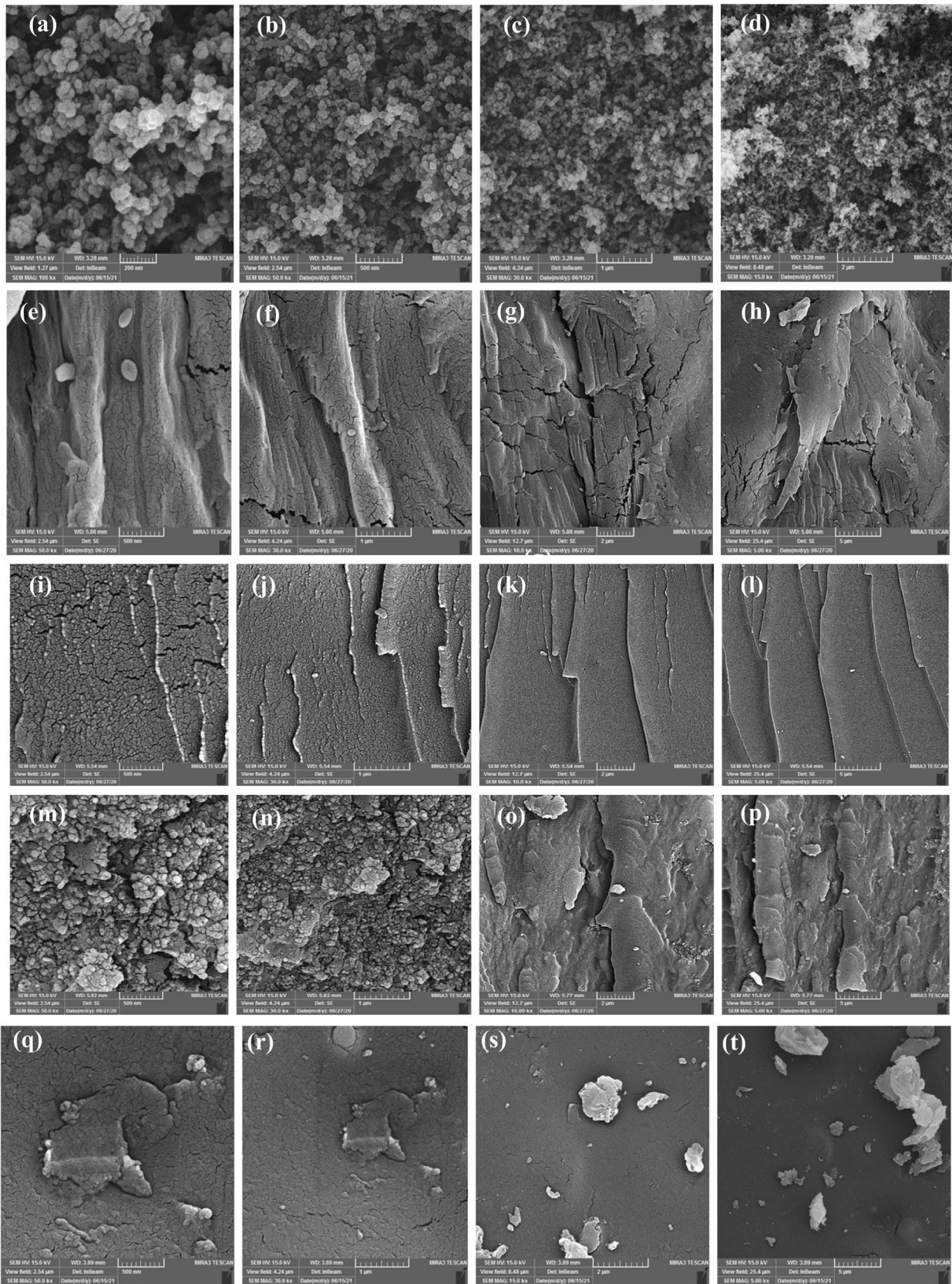


Fig. 2 SEM images of **a–d** CB, **e–h** CMC, **i–l** Hyd, **m–p** Hyd/CB, and **q–t** Hyd/CB after MB adsorption at different magnification

Results and Discussion

FTIR Spectra Analysis

FTIR spectra of CMC, AAm, CB, Hyd, and Hyd/CB are depicted in Fig. 1a and b. The characteristics peaks were observed in the FTIR spectrum of CMC at 3460, 2916, 1608, 1263, and 1056 cm^{-1} which is assigned to the stretching bands of $-\text{OH}$, $-\text{CH}$, $-\text{C}=\text{O}$, $\text{C}-\text{O}$, and $\text{C}-\text{O}-\text{C}$, respectively [27, 28]. For pure AAm monomer, the adsorption peaks at 3369, 3188, 2814, 1674, and 1430 can be corresponded to asymmetric stretching of $-\text{NH}$, symmetric stretching of $-\text{NH}$, stretching vibrations of $-\text{CH}$, $-\text{C}=\text{O}$, and $-\text{C}-\text{N}$, respectively [29]. In the FTIR spectrum of Hyd, the peaks at wavenumbers of 3427, 2920, 1697, 1552, 1263, and 1055 cm^{-1} were related to the overlapping of $-\text{OH}$ and $-\text{NH}$ bands, $-\text{CH}$, $-\text{C}=\text{O}$, $-\text{NH}$ (bending vibrations), $-\text{C}-\text{O}$ and $-\text{C}-\text{O}-\text{C}-$ bands, respectively [30]. The peak intensity of $-\text{OH}$ group of CMC was reduced in FTIR spectrum of Hyd because of participation this functional group in the free radical polymerization process for formation of hydrogel. Also, intensity of $-\text{C}=\text{O}$ peak of CMC and AAm was reduced after grafting polymerization and was shifted from 1607 and 1674 cm^{-1} to 1697 cm^{-1} . The small peak at wavenumber of 1458 cm^{-1} can be assigned to $-\text{C}-\text{N}$ vibrations of AAm which indicates successful grafting of AAm onto the CMC backbone [31, 32]. The FTIR spectrum of CB demonstrates absorption bands at 3438, 2910, 1778, and 1246 cm^{-1} which are assigned to $-\text{OH}$, $-\text{CH}$, $-\text{C}=\text{O}$, and $-\text{C}-\text{O}$, respectively. FTIR spectrum of Hyd/CB was almost identical to Hyd which demonstrated the physical interaction of these nanoparticles with polymeric chains.

Thermogravimetric Analysis (TGA)

TGA curves of CB, Hyd, and Hyd/CB are demonstrated in Fig. 1c. As shown in Fig. 1c, the decomposition of samples

happens in four stages. In the first step, the minor weight loss of 10% occurs in the temperature range of 35–90 °C which is related to moisture and water evaporation. The second degradation step happens due to the breakage of $\text{C}-\text{O}-\text{C}$ bands in CMC chains and dehydration of saccharide rings. The third degradation step which happens in the temperature range of 320–600 °C for CMC, 408–700 °C for Hyd, and 420–700 °C for Hyd/CB can be related to the decomposition of amide side and carboxyl groups. In the fourth step, the thermal decomposition of samples is related to the breakage of the polymer chain and the destruction of the hydrogel network. In this step, lower weight loss is observed for Hyd/CB nanocomposite hydrogel which demonstrates improvement of thermal stability of hydrogel by the addition of CB nanoparticles. Also, the higher char yield for Hyd/CB (30%) in comparison to CMC (22%) and Hyd (24%) verified this result. These findings are in accordance with the results of other researchers [8].

X-ray Diffraction Analysis (XRD)

XRD analysis was applied to determine the crystalline and amorphous nature of CMC, CB, Hyd, and Hyd/CB. As depicted in Fig. 1d, CMC has a relatively sharp peak around $2\theta = 20^\circ$ which demonstrates its semi-crystalline structure [33]. In the XRD pattern of CB, two relatively sharp peaks were presented at 2θ of 25.4° and 42.5° which are assigned to (002) reflection and the (10) band. A broad peak was observed around 24° in the XRD pattern of Hyd which demonstrates that the semi-crystalline structure of CMC was destroyed after grafting of P(AAm). In the XRD pattern of Hyd/CB, a relatively small peak was observed around 25° which overlapped with the broad peak of Hyd demonstrating that Hyd/CB has a relative crystalline structure due to the presence of CB nanoparticles.

Fig. 3 Effect of **a** weight percentage of AAm to the total weight, and **b** weight percentage of CB on removal efficiency at pH 7, dose 1.5 g/L, initial concentration 10 mg/L, contact time 60 min, temperature 25 °C, and mixing speed 400 rpm

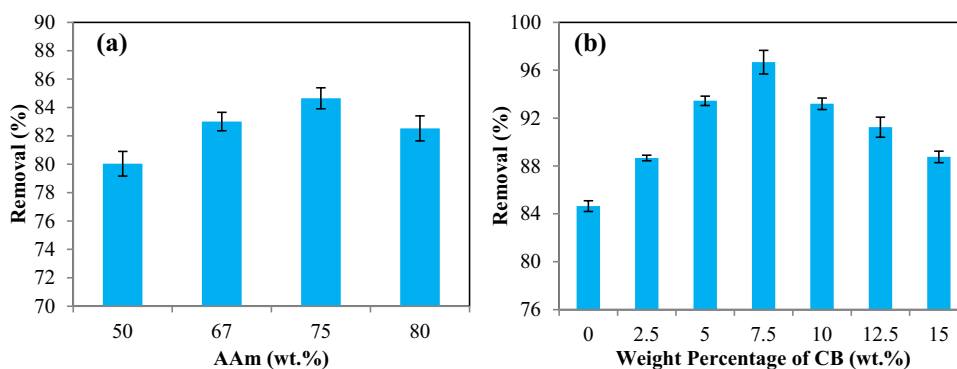
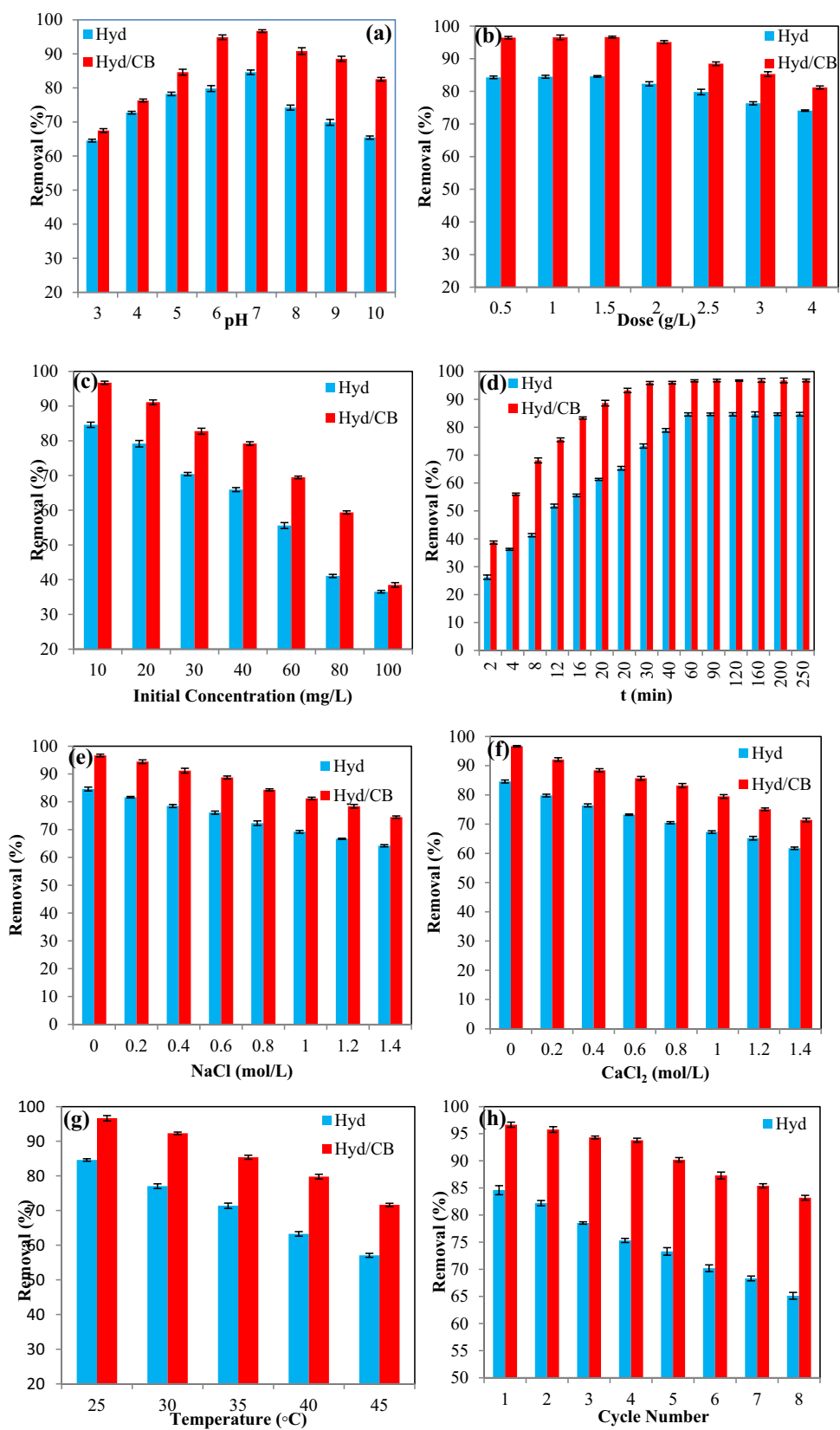


Fig. 4 Effect of **a** pH (dose 1 g/L, initial concentration 10 mg/L, contact time 60 min, temperature 25 °C, and mixing speed 400 rpm), **b** dose (pH 7, initial concentration 10 mg/L, contact time 60 min, temperature 25 °C, and mixing speed 400 rpm), **c** initial concentration (pH 7, dose 1 g/L, contact time 60 min, temperature 25 °C, and mixing speed 400 rpm), **d** contact time (pH 7, dose 1 g/L, initial concentration 10 mg/L, temperature 25 °C, and mixing speed 400 rpm), **e** NaCl, **f** CaCl₂, **g** temperature (pH 7, dose 1 g/L, initial concentration 10 mg/L, contact time 60 min, and mixing speed 400 rpm) on removal efficiency, and **h** Reusability



BET Analysis

The BET surface area, total pore volume, and mean pore diameter were determined using the measurement of N₂ adsorption and desorption. Isotherm curves of CB, Hyd, and Hyd/CB were shown in Fig. 1e and f. All mentioned samples have IV-type hysteresis loop based on IUPAC classification revealing mesoporous structure. For CB, BET surface area, total pore volume, and mean pore diameter were calculated to be 73.27 m²/g, 0.1902 cm³/g, and 10.381 nm, respectively. As shown in Fig. 1f, the amount N₂ adsorption and desorption for Hyd/CB is higher than Hyd which arises from the capability of CB to bond with polymer chains leading to a finer porous structure. BET surface area, total pore volume, and mean pore diameter were computed to be 0.92 m²/g, 0.00236 cm³/g, 8 nm, for Hyd, respectively, and 2.0665 m²/g, 0.0041376 cm³/g, and 10.254 nm for Hyd/CB, respectively. Based on the obtained results, incorporation of CB into Hyd matrix enhances BET surface area, total pore volume, and mean pore diameter so it was anticipated that Hyd/CB will have good performance in the decontamination of MB in comparison with Hyd.

Scanning Electron Microscopy (SEM) Analysis

The morphology of CB, CMC, Hyd, and Hyd/CB nanocomposite hydrogel is depicted in Fig. 2 (a–p) with different magnifications. Agglomeration of spherical particles of CB can be seen in Fig. 2a–d. According to Fig. 2e–h, some cracks can be seen in the CMC structure. As depicted in Fig. 2i–l, the grafting of P(AAm) and crosslinking with MBA led to the formation of heterogeneous and irregular surfaces with interconnected pores. The porous structure facilitates the diffusion of dye molecules to adsorbent structures and their accessibility to functional groups. Figure 2m–p demonstrates that Hyd/CB has a rougher surface than Hyd and the incorporation of CB enhances the porosity of the hydrogel matrix so higher removal efficiency can be expected for nanocomposite hydrogel. As depicted in Fig. 2q–s, the surface of Hyd/CB after MB adsorption gets smoother due to the filling of pores of the adsorbent with dye molecules.

The Influence of Different Parameters on MB Removal

Influence of Weight Ratio of AAm to CMC and CB Content

As shown in Fig. 3a, the weight percentage of AAm to total weight has a significant effect on the removal efficiency of hydrogels. When the weight ratio of AAm varied from 50 to 75 wt%, the removal efficiency was increased from 80.41 to 84.65%. By altering the weight percentage of AAm to total weight from 75 to 80 wt%, the removal efficiency was

decreased to 82.53% which can be related to the decrement of the grafting ratio by increasing the viscosity of the polymerization medium. The effect of CB content on the removal efficiency of Hyd is demonstrated in Fig. 3b. By increasing the weight percentage of CB from 0 to 7.5 wt%, the removal efficiency was increased from 84.5 to 96.68% then it decreased. By increasing CB content, the electrostatic repulsion between –COO[−] of CB and CMC enhances so the adsorbent structure is expanded leading to more dye diffusion. In addition, the electrostatic attraction between adsorbent and cationic dye molecules is promoted by increasing CB content. Further increase of CB leads to the decrement in removal efficiency which results from the act of nanoparticles as cross-linkers and filling of pores of adsorbents due to aggregation of CB particles.

Influence of pH

pH is a significant factor in the adsorption process that affects the surface charge of adsorbents and dye solutions. The effect of pH on the removal efficiency of Hyd and Hyd/CB is depicted in Fig. 4a. By increasing pH from 3 to 7, the removal efficiency was increased from 64.53 to 84.6% for Hyd and from 67.5 to 96.68% for Hyd/CB due to increment of electrostatic attraction between carboxyl groups of CMC and CB and cationic dye. By increasing pH from 7 to 10, the removal efficiency of both adsorbents was almost constant. In acidic pH, low removal efficiency is related to competition between dye molecules and H⁺ ions to sorption to active sites of adsorption and weak electrostatic attraction between cationic dye and low negatively charged adsorbent [34].

Influence of Adsorbent Dose

The effect of adsorbent dose on the removal efficiency of Hyd and Hyd/CB is depicted in Fig. 4b. It can be seen that the removal efficiency is increased when the adsorbents dose increases up to 1.5 g/L then it remains constant. By increasing the adsorbents dose, the number of the active site of adsorbents and surface area increases so the interactions between adsorbents and MB dye molecules are enhanced [35, 36]. For further experiments, the value of 1.5 g/L is selected as the optimum dose for both adsorbents.

Influence of Initial Concentration

Initial concentration as one of the significant factors of the decontamination process can have a significant effect on the removal efficiency and adsorption capacity. The initial concentration provides the driving force of mass transfer between dye solution and adsorbent and represses the mass transfer resistance. In the current study, the impact of initial concentration on MB removal was studied in the

Fig. 5 Curves of linear kinetic models **a** quasi-first-order, **b** quasi-second-order, **c** Temkin, and **d** IPD for Hyd and Hyd/CB

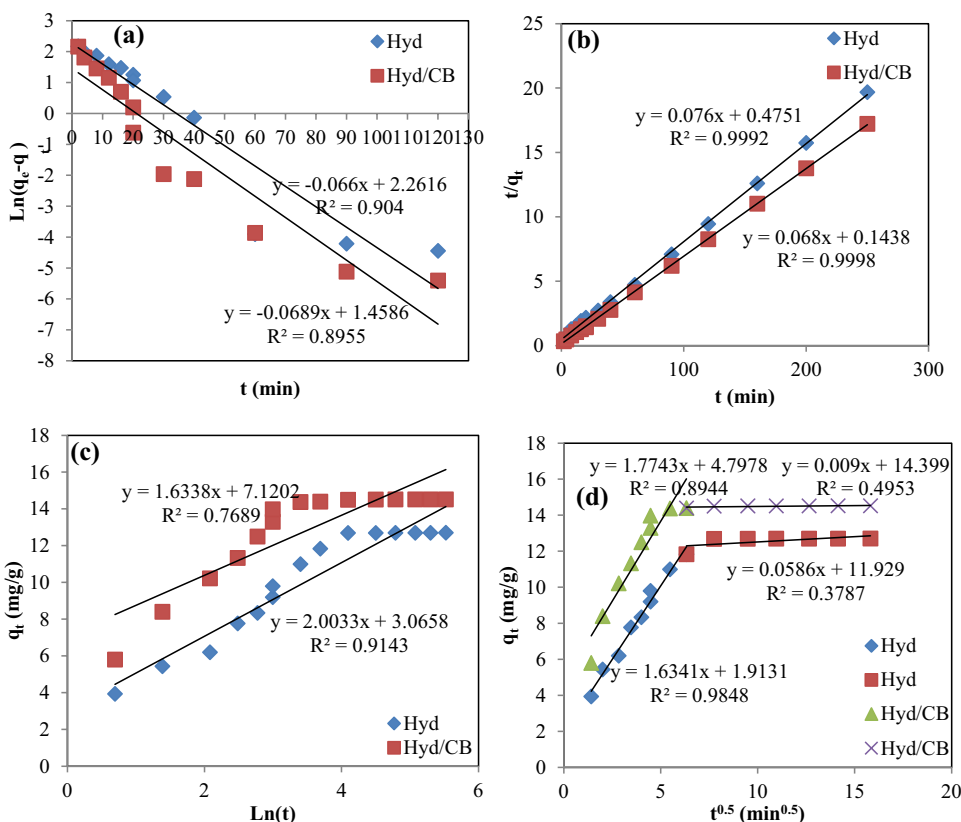


Table 2 Kinetic parameters for MB adsorption onto Hyd and Hyd/CB (pH 7, initial concentration of dyes 10 mg/L, adsorbent dose 1.5 g/L, temperature 25 °C, and mixing speed 400 rpm)

Kinetic model	Adsorbent		Kinetic model	Adsorbent	
	Hyd	Hyd/CB		Hyd	Hyd/CB
Quasi-first-order			Elovich		
$q_{e,cal}$ (mg/g)	9.598	4.299	α (mg/g min)	9.255	127.608
k_1 (min ⁻¹)	0.066	0.0689	β (g/mg)	0.499	0.612
R^2	0.904	0.895	R^2	0.914	0.7689
Quasi-second-order			IPD		
$q_{e,cal}$ (mg/g)	13.157	14.71	$k_{i,1}$ (mg/g min ^{0.5})	1.6341	1.7743
k_2 (g/mg min)	0.012	0.0321	C_1 (mg/g)	1.9131	4.7978
$q_{e,exp}$ (mg/g)	12.71	14.52	R^2	0.9848	0.8944
R^2	0.99	0.99	$k_{i,2}$ (mg/g min ^{0.5})	0.0586	0.0009
			C_2 (mg/g)	11.929	14.399
			R^2	0.3787	0.4953

range of 10–100 mg/L, and obtained results are depicted in Fig. 4c. With the increase of initial concentration from 10 to 80 mg/L, the removal efficiency was decreased from 84.59 to 36.55% for Hyd and from 96.73 to 38.48% for Hyd/CB due to saturation of active sites of adsorbents [37].

Influence of Contact Time

The dependency of MB adsorption rate on the contact time was evaluated in the range of 2–250 min at pH of 7, initial

concentration of 10 mg/L, adsorbent dose of 1.5 g/L, and temperature of 25 °C. As depicted in Fig. 4d, the removal efficiency increased with the increment of contact time from 2 to 60 min due to the vacancy of the sorption site of adsorbents [38]. After 60 min, the adsorption process reached equilibrium and a further increase in contact time hasn't effect on removal efficiency. The equilibrium removal efficiency for nanocomposite hydrogel is 96.66% which is 12.06% higher than the removal efficiency of the hydrogel.

Influence of Ionic Strength

The ionic strength and co-existing ions are two major factors that affect the performance of adsorbents. In this regard, NaCl and CaCl₂ salts in the concentration range of 0–1.4 mol/L were selected to assess the interference effect of Na⁺, Ca²⁺ ions, and MB molecules to sorption to adsorption sites, and findings were demonstrated in Fig. 4e and f. The obtained results showed that the removal efficiency of synthesized adsorbents decreased by increasing the concentration of salts which is assigned to increment of competition between Na⁺ and Ca²⁺ ions and MB molecules to sorption to active sites [20]. In addition, the decrement of the removal performance of adsorbents in presence of Ca²⁺ ions was higher than Na⁺ relating to act of Ca²⁺ as a crosslinker which limits the expansion of hydrogels network [8].

Influence of Temperature

The influence of temperature on the removal efficiency was assessed when the temperature was raised from 25 to 45 °C. As shown in Fig. 4g, the removal efficiency decreased from 96.66 to 71.65% for nanocomposite hydrogel and 84.59 to 57.09% for hydrogel as the temperature was changed from 25 to 45 °C. The decrement in removal efficiency with the increase in temperature can be related to the separation of MB molecules from the adsorbent's surface and some structural changes in adsorbents [8].

Reusability

From the economical view of point, one adsorbent should have reusability in the different adsorption–desorption cycles without a significant loss in the removal performance. For this purpose, the reusability of synthesized adsorbents was investigated in eight successive adsorption–desorption cycles. Desorption of MB from adsorbents was performed by immersing them in 1 M HNO₃ solution for 4 h then they were washed several times with distilled water to prepare them for the next adsorption cycle. As depicted in Fig. 4h,

the removal efficiency of Hyd and Hyd/CB were nearly constant in two and four cycles, respectively then it decreased. The decrement in removal efficiency can be attributed to the morphological changes and blocking of active sites of adsorbents [39]. Finally, it can be concluded that the synthesized adsorbents can be applied economically and potentially for the removal of MB from an aqueous solution.

Kinetics Study

To evaluate the kinetic behavior of MB adsorption, quasi-first-order (Eq. 3), quasi-second-order (Eq. 4), Elovich (Eq. 5), and intra-particle diffusion (IPD, Eq. 6) models were used which were presented in the following equations.

$$\ln(q_e - q_t) = \ln q_{e,cal} - k_1 t \quad (3)$$

$$\frac{t}{q_t} = \frac{t}{q_e} + \frac{1}{k_2 q_e^2} \quad (4)$$

$$q_t = \frac{1}{\beta} \ln(t) + \frac{1}{\beta} \ln(\alpha\beta) \quad (5)$$

$$q_t = k_{i,d} t^{0.5} + C_i \quad (6)$$

where q_e , $q_{e,cal}$ (mg/g), k_1 (min⁻¹) and k_2 (g/mg min) represent experimental equilibrium adsorption capacity, theoretical equilibrium adsorption capacity, rate constants of PFO, and PSO models, respectively. In the Elovich model, α (mg/g min) represents the initial absorbance and β (g/mg) reflects the desorption constant related to surface coverage, and activation energy of chemisorption [40]. k_i (mg/g min^{0.5}) and C_i (mg/g) are intra-particle diffusion rate constant and the intercept of q_t vs $t^{0.5}$ plot depicting boundary layer effect, respectively [41]. The fitting results based on the data in Fig. 4d are shown in Fig. 5a–d and calculated parameters of kinetic models are tabulated in the Table 2. Comparison of R^2 values of kinetic models showed that the quasi-second-order model has the nearest value to 1 showing the rate of

Table 3 Isotherm parameters for MB adsorption onto Hyd and Hyd/CB samples (pH 7, contact time 60 min, adsorbent dose 1 g/L, temperature 25 °C, and mixing speed 400 rpm)

Isotherm model	Adsorbent		Isotherm model	Adsorbent	
	Hyd	Hyd/CB		Hyd	Hyd/CB
Langmuir			Temkin		
q_m (mg/g)	26.247	27.32	K_T (L/g)	2.01	31.836
k_1 (L/mg)	0.155	0.9196	b (J/mol)	486.195	644.3
R^2	0.99	0.9833	R^2	0.9771	0.849
Freundlich			Dubinin-Radushkevich		
n	2.63	4.019	q_s (mg/g)	18.976	21.658
K_F (mg/g.(L/mg) ^{1/n})	5.6865	11.57	E_a (kJ/mol)	0.79	4.082
R^2	0.938	0.9385	R^2	0.8185	0.6762

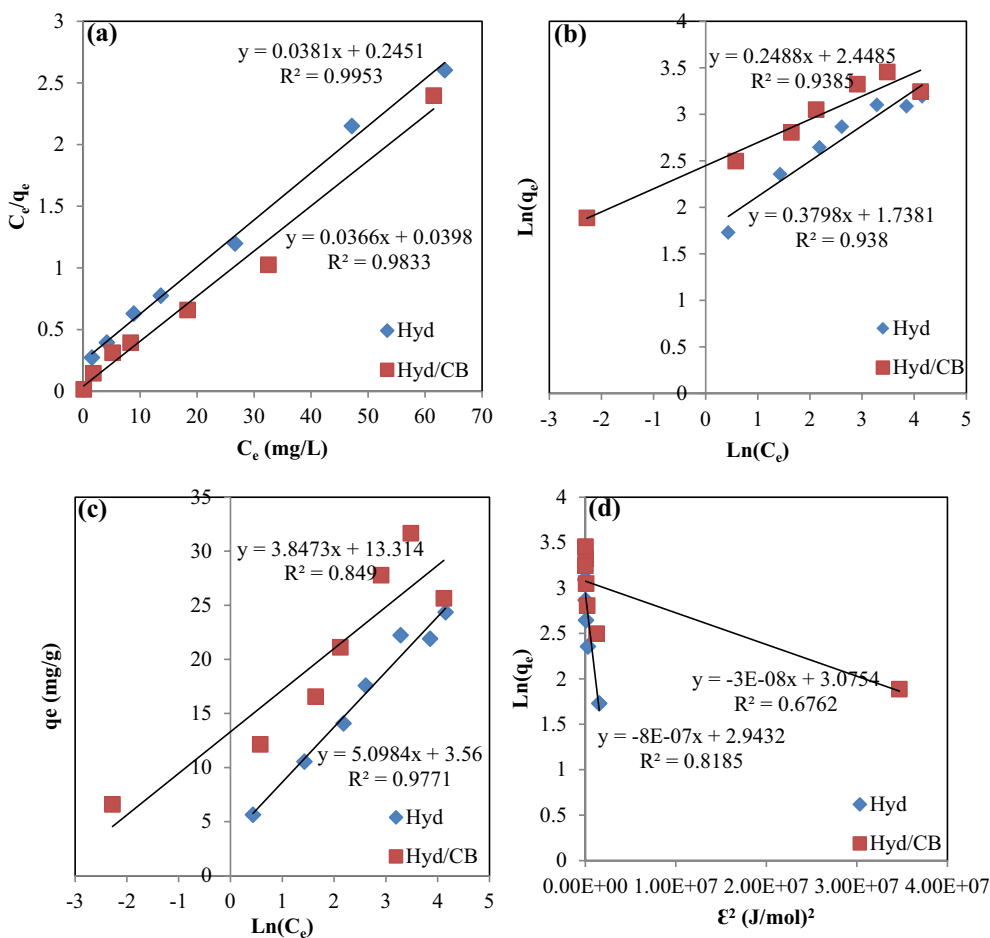


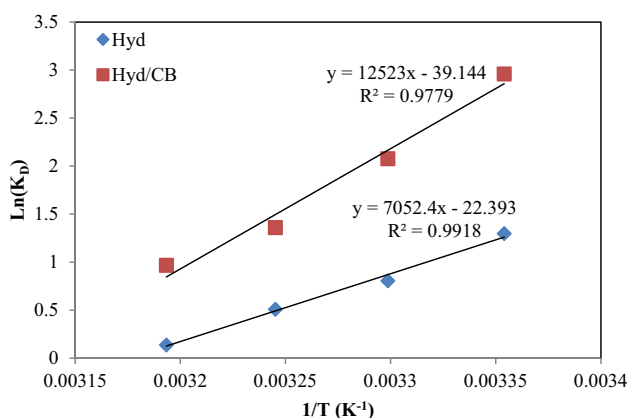
Fig. 6 Curves of linear isotherm models for Hyd and Hyd/CB nanocomposite hydrogel **a** Langmuir, **b** Freundlich, **c** Temkin, and **d** Dubinin-Radushkevich

Table 4 Comparison of maximum monolayer adsorption capacity of Hyd and Hyd/CB samples with other adsorbents used in MB adsorption

Adsorbent	Initial concentration	Q_m (mg/g)	References
N-isopropylacrylamide	10–50	8.5	[44]
N-isopropylacrylamide/itaconic acid	10–50	17.52	[44]
N-isopropylacrylamide/itaconic acid/pumice	10–50	22.18	[44]
Carboxymethyl cellulose/k-carrageenan/activated montmorillonite	10–500	10.75	[45]
Carboxymethyl cellulose coated $Fe_3O_4@SiO_2$ magnetic nanoparticles	100	17.5	[46]
Alginate/almond peanut bio composite	25–100	22.8	[47]
H_2SO_4 crosslinked magnetic chitosan nanocomposite bead	–	20.408	[48]
Hyd	10–100	26.247	This work
Hyd/CB	10–100	27.32	This work

Table 5 Thermodynamic parameters of MB adsorption to Hyd and Hyd/CB samples

Adsorbent	T(°C)	ΔG° (KJ/mol)	ΔH° (KJ/mol)	ΔS° (KJ/mol K)
Hyd	25	-3.217	-58.633	-0.186
	30	-1.999		
	35	-1.263		
	40	-0.344		
	45	-0.296		
Hyd/CB	25	-7.336	-104.129	-0.325
	30	-5.151		
	35	-3.373		
	40	-2.4		
	45	-1.293		

**Fig. 7** Plot of $\text{Ln}(K_D)$ vs $1/T$

MB adsorption is controlled by chemisorption. MB molecule's migration during the adsorption process was assessed by the IPD model. According to Fig. 5d, MB adsorption occurs in two stages including diffusion of dye molecules from bulk to the adsorbent surface (first stage) and diffusion of dye molecules through pores (second stage). In addition to intra-particle diffusion, boundary layer diffusion controls MB adsorption rate because the fitting curve intercept doesn't pass through the origin [38, 42].

Isotherms Study

The four most common isotherm models include Langmuir (Eq. 7), Freundlich (Eq. 8), Temkin (Eq. 9), and Dubinin-Radushkevich (Eq. 10) models are applied to understand the distribution of MB molecules at aqueous/adsorbents surface [43]. The mathematical equations of these models are represented as follows.

$$\frac{C_e}{q_e} = \frac{C_e}{q_m} + \frac{1}{K_L q_m} \quad R_L = \frac{1}{1 + K_L C_i} \quad (7)$$

$$\text{Ln}(q_e) = \text{Ln}(K_F) = \frac{1}{n} \text{Ln}(C_e) \quad (8)$$

$$q_e = B \text{Ln}(K_T) + B \text{Ln}(C_e) \quad B = \frac{RT}{b} \quad (9)$$

$$\text{Ln}(q_e) = \text{Ln}(q_s) - \beta \varepsilon^2, \quad \varepsilon = RT \text{Ln} \left(1 + \frac{1}{C_e} \right), \quad E_a = \frac{1}{\sqrt{2\beta}} \quad (10)$$

where q_m , and K_L (mg/L) denote the Langmuir constant and maximum monolayer adsorption capacity, respectively. K_F (mg/g (L/mg)^{1/n}) and n are Freundlich constants, K_T (L/g) demonstrates Temkin equilibrium binding constant, and B is a constant related to the heat of sorption. In Dubinin-Radushkevich (D-R) isotherm model, q_s (mg/g), β (mol²/J²), ε (J/mol), and E_a (kJ/mol) are theoretical saturation adsorption capacity, Dubinin-Radushkevich constant, Polanyi potential, and mean adsorption energy, respectively. Equilibrium data of MB adsorption are fitted by mentioned models (Fig. 6) and their parameters are tabulated in the Table 3. The correlation factor (R^2) of the Langmuir model is higher than other models depicting monolayer adsorption of MB molecules occurring on homogenous adsorption surface [2]. The maximum monolayer adsorption capacity is 26.247 and 27.32 mg/g for Hyd and Hyd/CB, respectively. The higher adsorption capacity of Hyd/CB is related to providing higher surface area and more adsorption sites which are provided by CB nanoparticles. The values of separation factor (R_L) for both adsorbents are founded to be between 0 and 1 revealing that the MB removal process is desirable [38]. The values of this factor for Hyd/CB are lower than Hyd indicating more desirability of MB adsorption onto nanocomposite hydrogel.

To evaluate the performance of synthesized adsorbents, a comparison study is performed based on maximum monolayer adsorption. As depicted in Table 4, synthesized adsorbents show good performance in the adsorption of MB from aqueous solution so they can be used as efficient adsorbents for the remediation of MB from wastewater.

Thermodynamic Study

To understand the nature and feasibility of the decontamination process, thermodynamic parameters are determined in the temperature range of 25–45 °C. Changes in Gibbs free energy (ΔG°), change in enthalpy (ΔH°), and change in entropy (ΔS°) are calculated using Van't Hoff formula (Eq. 11), and obtained results are presented in Table 5.

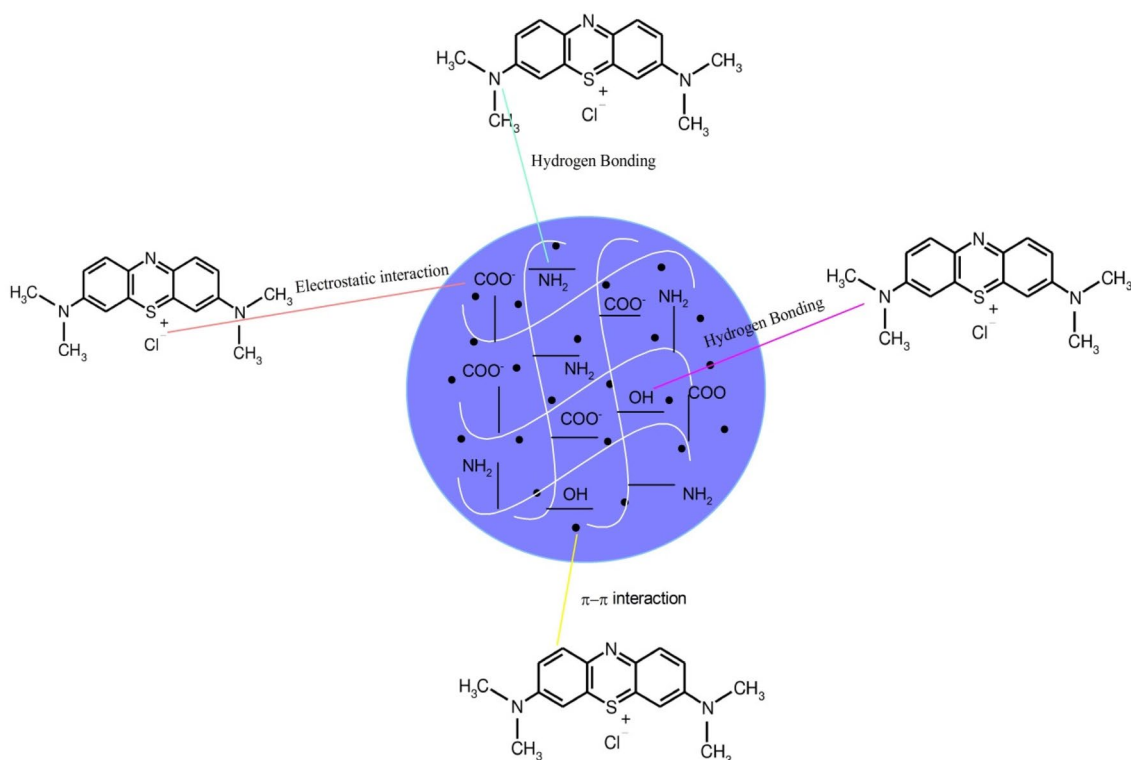


Fig. 8 Scheme of MB adsorption mechanism by Hyd/CB nanocomposite hydrogel

$$\ln(K_D) = -\frac{\Delta H^\circ}{RT} + \frac{\Delta S^\circ}{R} \quad K_D = \frac{q_e}{C_e} \quad (11)$$

$$\Delta G^\circ = -RT \ln(K_D) \quad (12)$$

where K_D is the equilibrium constant, R (8.314 J/mol.K) is the global gas constant, and T (K) is the absolute temperature. The values of ΔH° and ΔS° are computed from the slope and intercept of the Van't Hoff equation (Eq. 11), respectively which is plotted in Fig. 7.

The adsorption of MB onto both adsorbents is spontaneous and favorable due to negative values of ΔG° and the adsorption process occurs physically due to the values of ΔG° for both adsorbents being in the range of -20 – 0 kJ/mol [2, 4, 49]. Decrement of the negative values of ΔG° with rising temperature demonstrates decrement in the spontaneity of the decontamination process [35]. The values of ΔH° for both adsorbents are negative depicting the exothermic nature of the adsorption process. The calculated values of ΔS° for both adsorbents are negative so random collisions between MB molecules and the surface of adsorbents decrease during the decontamination process.

Adsorption Mechanism

A proposed adsorption mechanism to Hyd/CB nanocomposite hydrogel is illustrated in Fig. 8. Based on the chemical structure of MB and nanocomposite hydrogel, it can be concluded that electrostatic attraction between cationic dye and carboxyl groups of adsorbents, H-bonding between $-\text{OH}$ and $-\text{NH}_2$ groups of adsorbent and nitrogen of dye, and π - π interaction between aromatic rings of MB and CB of adsorbent is the main mechanism of MB adsorption.

Conclusion

In the present study, CMC grafted poly(acrylamide) hydrogel was synthesized successfully to remediation of MB from an aqueous solution. To enhance the performance of synthesized adsorbent, various contents of CB nanoparticles were incorporated into the hydrogel matrix and its content was optimized carefully. Different analyses such as FTIR, TGA, XRD, BET, and SEM were performed to characterize the surface and structural properties of adsorbents. The results of the TGA analysis indicated that the thermal stability of hydrogel improves with the incorporation of CB. The kinetic and isotherm study showed that kinetic and isotherm

data best fit to quasi-second-order and Langmuir models, respectively. The maximum adsorption capacity (q_m) of MB was calculated to be 26.247 and 27.32 mg/g for Hyd and Hyd/CB, respectively revealing that the performance of Hyd/CB in MB removal is higher than the hydrogel. The thermodynamic study showed that the adsorption process is spontaneous, exothermic, and entropy decreased. Finally, it can be concluded that the synthesized adsorbents have potential application in removing MB from an aqueous solution. For future work, it can be proposed that the simultaneous selective separation of dyes from aqueous solutions will investigate because the presence of mixtures of dyes in wastewater is the main problem for the industrial application of adsorbents.

Author Contributions EG performed the samples' synthesis, and collected test data; SJP designed the study, interpreted the results, and revised the manuscript critically for important intellectual content; PMP drafted the manuscript, and HA advising on Conceptualization. All authors approve the final version of the manuscript and agree to be accountable for all aspects of the work.

Funding This research was conducted in the absence of any commercial or financial relationships that could be construed as a potential conflict of interest.

Declarations

Conflict of interest This research could be construed as a potential conflict of interest. Thus, the authors declare no conflict of interest.

References

- Wang W, Wang J, Zhao Y, Bai H, Huang M, Zhang T, Song S (2020) High-performance two-dimensional montmorillonite supported-poly(acrylamide-co-acrylic acid) hydrogel for dye removal. *Environ Pollut* 257:113574
- Kang S, Zhao Y, Wang W, Zhang T, Chen T, Yi H, Rao F, Song S (2018) Removal of methylene blue from water with montmorillonite nanosheets/chitosan hydrogels as adsorbent. *Appl Surf Sci* 448:203–211
- Mohammadzadeh Pakdel P, Peighambaroust SJ (2018) A review on acrylic based hydrogels and their applications in wastewater treatment. *J Environ Manag* 217:123–143
- Dalalibera A, Vilela PB, Vieira T, Becegato VA, Paulino AT (2020) Removal and selective separation of synthetic dyes from water using a polyacrylic acid-based hydrogel: characterization, isotherm, kinetic, and thermodynamic data. *J Environ Chem Eng* 8(5):104465
- Sinha V, Chakma S (2019) Advances in the preparation of hydrogel for wastewater treatment: a concise review. *J Environ Chem Eng* 7(5):103295
- Mohammadzadeh Pakdel P, Peighambaroust SJ (2018) Review on recent progress in chitosan-based hydrogels for wastewater treatment application. *Carbohydr Polym* 201:264–279
- Abdolhosseinzadeh M, Peighambaroust SJ, Erfan-Niya H, Mohammadzadeh Pakdel P (2018) Swelling and auramine-O adsorption of carboxymethyl cellulose grafted poly (methyl methacrylate)/cloisite 30B nanocomposite hydrogels. *Iran Polym J* 27(10):807–818
- Mohammadzadeh Pakdel P, Peighambaroust SJ, Arsalani N, Aghdasinia H (2022) Safranin-O cationic dye removal from wastewater using carboxymethyl cellulose-grafted-poly(acrylic acid-co-itaconic acid) nanocomposite hydrogel. *Environ Res* 212:113201
- Peighambaroust SJ, Aghamohammadi-Bavil O, Foroutan R, Arsalani N (2020) Removal of malachite green using carboxymethyl cellulose-g-polyacrylamide/montmorillonite nanocomposite hydrogel. *Int J Biol Macromol* 159:1122–1131
- Varaprasad K, Jayaramudu T, Sadiku ER (2017) Removal of dye by carboxymethyl cellulose, acrylamide and graphene oxide via a free radical polymerization process. *Carbohydr Polym* 164:186–194
- Sinha V, Chakma S (2020) Synthesis and evaluation of CMC-g-AMPS/Fe/Al/AC composite hydrogel and their use in fluoride removal from aqueous solution. *Environ Technol Innov* 17:100620
- Khan SA, Khan TA (2021) Clay-hydrogel nanocomposites for adsorptive amputation of environmental contaminants from aqueous phase: a review. *J Environ Chem Eng* 9(4):105575
- Rahmatpour A, Soleimani P, Mirkani A (2022) Eco-friendly poly(vinyl alcohol)/partially hydrolyzed polyacrylamide/graphene oxide semi-IPN nanocomposite hydrogel as a reusable and efficient adsorbent of cationic dye methylene blue from water. *React Funct Polym* 175:105290
- Oladipo AA, Gazi M (2015) Microwaves initiated synthesis of activated carbon-based composite hydrogel for simultaneous removal of copper(II) ions and direct red 80 dye: a multi-component adsorption system. *J Taiwan Inst Chem Eng* 47:125–136
- Soltani RDC, Mahmoudi M, Boczkaj G, Khataee A (2020) Activation of peroxymonosulfate using carbon black nano-spheres/calcium alginate hydrogel matrix for degradation of acetaminophen: Fe3O4 co-immobilization and microbial community response. *J Ind Eng Chem* 91:240–251
- Boukhalfa N, Boutahala M, Djebri N, Idris A (2019) Maghemite/alginate/functionalized multiwalled carbon nanotubes beads for methylene blue removal: adsorption and desorption studies. *J Mol Liq* 275:431–440
- Khan A, Alamry KA, Oves M, Althomali RH (2021) A facile and green approach for the fabrication of nano-biocomposites by reducing silver salt solution into silver nanoparticles using modified carboxymethyl cellulose for antimicrobial potential. *J Polym Res* 28(3):1–13
- Makhado E, Pandey S, Nomngongo PN, Ramontja J (2018) Preparation and characterization of xanthan gum-cl-poly(acrylic acid)/o-MWCNTs hydrogel nanocomposite as highly effective re-usable adsorbent for removal of methylene blue from aqueous solutions. *J Colloid Interface Sci* 513:700–714
- Makhado E, Pandey S, Ramontja J (2018) Microwave assisted synthesis of xanthan gum-cl-poly (acrylic acid) based-reduced graphene oxide hydrogel composite for adsorption of methylene blue and methyl violet from aqueous solution. *Int J Biol Macromol* 119:255–269
- Foroutan R, Peighambaroust SJ, Latifi P, Ahmadi A, Alizadeh M, Ramavandi B (2021) Carbon nanotubes/ β -cyclodextrin/MnFe2O4 as a magnetic nanocomposite powder for tetracycline antibiotic decontamination from different aqueous environments. *J Environ Chem Eng* 9(6):106344
- Chen Y, Xiang Z, Wang D, Kang J, Qi H (2020) Effective photocatalytic degradation and physical adsorption of methylene blue using cellulose/GO/TiO₂ hydrogels. *RSC Adv* 10(40):23936–23943

22. Arikal D, Kallingal A (2021) Photocatalytic degradation of azo and anthraquinone dye using TiO₂/MgO nanocomposite immobilized chitosan hydrogels. *Environ Technol* 42(15):2278–2291
23. Althomali RH, Alamry KA, Hussein MA, Guedes R (2022) Highly sensitive detection analytical performance of 2-nitrophenol pollution in various water samples via polyaniline/sulfation carboxymethylcellulose/multi carbon nanotubes nanocomposite-based electrochemical sensor. *J Electrochem Soc* 169(4):046518
24. Pawlyta M, Rouzaud J-N, Duber S (2015) Raman microspectroscopy characterization of carbon blacks: spectral analysis and structural information. *Carbon* 84:479–490
25. Khodabakhshi S, Fulvio PF, Andreoli E (2020) Carbon black reborn: structure and chemistry for renewable energy harnessing. *Carbon* 162:604–649
26. Mittal H, Al Alili A, Morajkar PP, Alhassan SM (2021) GO crosslinked hydrogel nanocomposites of chitosan/carboxymethyl cellulose—a versatile adsorbent for the treatment of dyes contaminated wastewater. *Int J Biol Macromol* 167:1248–1261
27. Althomali RH, Alamry KA, Hussein MA, Khan A, Alosaimi AM (2021) A green nanocomposite based modified cellulose/TiO₂/Cinnamon bark for the reduction of toxic organic compounds using spectrophotometric technique. *J Market Res* 12:947–966
28. Althomali RH, Alamry KA, Hussein MA, Guedes RM (2022) Hybrid PANI@di-aldehyde carboxymethyl cellulose/ZnO nanocomposite modified glassy carbon electrode as a highly sensitive electrochemical sensor. *Diam Relat Mater* 122:108803
29. Tanwar A, Date P, Ottoor D (2021) ZnO NPs incorporated gelatin grafted polyacrylamide hydrogel nanocomposite for controlled release of ciprofloxacin. *Colloid Interface Sci Commun* 42:100413
30. Sharika T, Mohanan A (2021) Synthesis and swelling studies of poly (acrylamide-co-itaconic acid)/hydroxyapatite nanocomposite hydrogels. *Mater Today Proc* 41:744–751
31. Feng X, Wan J, Deng J, Qin W, Zhao N, Luo X, He M, Chen X (2020) Preparation of acrylamide and carboxymethyl cellulose graft copolymers and the effect of molecular weight on the flocculation properties in simulated dyeing wastewater under different pH conditions. *Int J Biol Macromol* 155:1142–1156
32. Foroutan R, Peighambaroust SJ, Hemmati S, Ahmadi A, Fallotta E, Ramavandi B, Bianchi CL (2021) Zn²⁺ removal from the aqueous environment using polydopamine/hydroxyapatite/Fe₃O₄ magnetic composite under ultrasonic waves. *RSC Adv* 11:27309–27321
33. Manikandan K, Yelilarasi A, Saravanakumar S, Althomali RH, Khan A, Abualnaja KM, Alhashmialameer D, Hussein M (2021) The effect of plasticizers on the polypyrrole-poly(vinyl alcohol)-based conducting polymer electrolyte and its application in semi-transparent dye-sensitized solar cells. *Membranes* 11(10):791
34. Verma A, Thakur S, Mamba G, Gupta RK, Thakur P, Thakur VK (2020) Graphite modified sodium alginate hydrogel composite for efficient removal of malachite green dye. *Int J Biol Macromol* 148:1130–1139
35. Eltaweil AS, Elgarhy GS, El-Subruiti GM, Omer AM (2020) Carboxymethyl cellulose/carboxylated graphene oxide composite microbeads for efficient adsorption of cationic methylene blue dye. *Int J Biol Macromol* 154:307–318
36. Althomali RH, Alamry KA, Hussein MA, Khan A, Al-Juaid SS, Asiri AM (2020) Modification of alginate acid for the removal of dyes from aqueous solutions by solid-phase extraction. *Int J Environ Anal Chem*. <https://doi.org/10.1080/03067319.2020.177277>
37. Safarzadeh H, Peighambaroust SJ, Mousavi S, Mohammadi R, Peighambaroust S (2022) Adsorption of methyl violet dye from wastewater using poly(methacrylic acid-co-acrylamide)/bentonite nanocomposite hydrogels. *J Polym Res*. <https://doi.org/10.1007/s10965-022-02956-0>
38. Foroutan R, Mohammadi R, Ahmadi A, Bikhbar G, Babaei F, Ramavandi B (2022) Impact of ZnO and Fe₃O₄ magnetic nanoscale on the methyl violet 2B removal efficiency of the activated carbon oak wood. *Chemosphere* 286:131632
39. Sakthivel M, Franklin DS, Sudarsan S, Chitra G, Sridharan TB, Guhanathan S (2018) Investigation on pH/salt-responsive multifunctional itaconic acid based polymeric biocompatible, antimicrobial and biodegradable hydrogels. *React Funct Polym* 122:9–21
40. Kalthori EM, Yetilmeszooy K, Uygur N, Zarrabi M, Shmeis RMA (2013) Modeling of adsorption of toxic chromium on natural and surface modified lightweight expanded clay aggregate (LECA). *Appl Surf Sci* 287:428–442
41. Pholosi A, Naidoo EB, Ofomaja AE (2020) Intraparticle diffusion of Cr(VI) through biomass and magnetite coated biomass: a comparative kinetic and diffusion study. *S Afr J Chem Eng* 32:39–55
42. Sayed A, Mahmoud GA, Said H, Diab AA (2022) Characterization and optimization of magnetic Gum-PVP/SiO₂ nanocomposite hydrogel for removal of contaminated dyes. *Mater Chem Phys* 280:125731
43. Wang J, Guo X (2020) Adsorption isotherm models: classification, physical meaning, application and solving method. *Chemosphere* 258:127279
44. Taşdelen B, Çifçi Dİ, Meriç S (2017) Preparation of N-isopropylacrylamide/itaconic acid/Pumice highly swollen composite hydrogels to explore their removal capacity of methylene blue. *Colloids Surf A* 519:245–253
45. Liu C, Omer AM, Ouyang X-K (2018) Adsorptive removal of cationic methylene blue dye using carboxymethyl cellulose/k-carrageenan/activated montmorillonite composite beads: isotherm and kinetic studies. *Int J Biol Macromol* 106:823–833
46. Zirak M, Abdollahiyan A, Eftekhari-Sis B, Saraei M (2017) Carboxymethyl cellulose coated Fe₃O₄@SiO₂ core-shell magnetic nanoparticles for methylene blue removal: equilibrium, kinetic, and thermodynamic studies. *Cellulose* 25:503–515
47. Hachi M, Chergui A, Selatnia A, Cabana H (2016) Valorization of the spent biomass of *Pleurotus mutilus* immobilized as calcium alginate biobeads for methylene blue biosorption. *Environ Process* 3:413–430
48. Mustafa I (2019) Methylene blue removal from water using H₂SO₄ crosslinked magnetic chitosan nanocomposite beads. *Microchem J* 144:397–402
49. Sharma S, Sharma G, Kumar A, AlGarni TS, Naushad M, Althoman ZA, Stadler FJ (2022) Adsorption of cationic dyes onto carrageenan and itaconic acid-based superabsorbent hydrogel: synthesis, characterization and isotherm analysis. *J Hazard Mater* 421:126729

Publisher's Note Springer Nature remains neutral with regard to jurisdictional claims in published maps and institutional affiliations.

Springer Nature or its licensor (e.g. a society or other partner) holds exclusive rights to this article under a publishing agreement with the author(s) or other rightsholder(s); author self-archiving of the accepted manuscript version of this article is solely governed by the terms of such publishing agreement and applicable law.